A chemical kinetic investigation on butyl formate oxidation: *ab-initio* calculations and experiments in a jet-stirred reactor

Aristotelis M. Zaras[1], Milán Szőri[2,3], Sébastien Thion[1,4], Pierre Van Cauwenberghe[1,4], Fiona Deguillaume[1,4], Zeynep Serinyel[1,4], Guillaume Dayma[1,4]† and Philippe Dagaut[1]

[1] CNRS-INSIS, Institut de Combustion, Aérothermique, Réactivité et Environnement 1C, Avenue de la recherche scientifique, 45071 Orléans cedex 2, France

[2] Institute of Chemistry, University of Miskolc, Miskolc-Egyetemváros, A/2, H-3515, Miskolc, Hungary

[3] Department of Chemical Informatics, Faculty of Education, University of Szeged, Boldogasszony sgt. 6, H-6725, Szeged, Hungary

[4] Université d'Orléans, 6 Avenue du Parc Floral, 45100 Orléans, France

†Corresponding author: guillaume.dayma@cnrs-orleans.fr

Abstract

Biofuels are expected to play a significant role in the quest for greener energy generation. In this perspective, esters produced from biomass are promising candidates. This work presents the first computational kinetic study on n-butyl formate (BF) oxidation by the OH radical under combustion conditions coupled to an experimental study in a jet-stirred reactor. Absolute rate constants for hydrogen abstraction reactions by the OH radical were calculated using the G3//MP2/aug-cc-pVDZ levels of theory in conjunction with statistical rate theory (TST). Subsequently, the fate of the butyl formate radicals was also investigated by calculating absolute rate constants for combustion relevant decomposition channels such as β-scission and hydrogen transfer reactions. The derived rate expressions were used in the presently developed detailed kinetic mechanism which was validated over experimental data obtained in a jet-stirred reactor at 10 atm and for 3 different mixtures (φ = 0.45, 0.9 and 1.8). Rate of production analyses were finally used to understand the oxidation kinetics of butyl formate over the temperature range 500–1300 K, and highlighted the importance of the unimolecular decomposition reactions of the fuel producing formic acid and 1-butene.

Keywords: kinetics, modeling, ab initio, butyl formate, jet stirred reactor

1. Introduction

Petroleum derived fuels are widely used in transportation and industry. Their combustion generates greenhouse gases, responsible for global warming. Added to the non-renewable nature of petroleum, one conceives the need for reducing the use of petroleum based fuels. An interesting alternative is the production of oxygenated fuels from biomass [1-4], as their combustion yields reduced emissions of carbon monoxide as well as soot from diesel engines [5, 6]. The kinetics of small esters such as methyl and ethyl formate has already been studied experimentally in flow reactors, shock tubes, and spherical bombs [7-9]. Similarly, n-butyl formate (BF) oxidation was also investigated by Vranckx et al. [10] who measured ignition delay times and laminar burning velocities of BF/air mixtures in various conditions. They also proposed a detailed kinetic mechanism, mainly based on estimations, to represent their data. However, rate constants for H-atom abstraction reactions of BF with H and HO_2 were computed by the same group using the B2KPLYP/aug-cc-pvtz//B3LYP/TZVP level of theory [11]. Despite their importance, hydrogen abstraction rate constants for BF + OH were estimated using site specific rate constant expressions for n-butanol + OH and ethyl-formate + OH reactions [10]. Only two experimental studies [12, 13] have been reported for the H-abstraction reactions by the OH radical, and these measurements were carried out at temperatures relevant to atmospheric chemistry (253 to 371K). Because of the lack of data on butyl formate oxidation, the aim of the current work is to develop a detailed kinetic mechanism based on theoretical calculations and new experiments at 10 atm performed in a jet-stirred reactor over the temperature range 500–1300 K.

2. Computational Methodology

Throughout this study, butyl formate will be referred to as BF, and its radicals as BFRn, where n indicates the carbon number on which the radical site is located, carbon #1 being the carbon of the ester function. The global minimum structure of BF was determined by Kopp et al. [11] and their geometry was used as the initial structure in our study. Geometry as well as carbon numbering are shown in Figure 1, which also illustrates the different pathways investigated for the theoretical study.

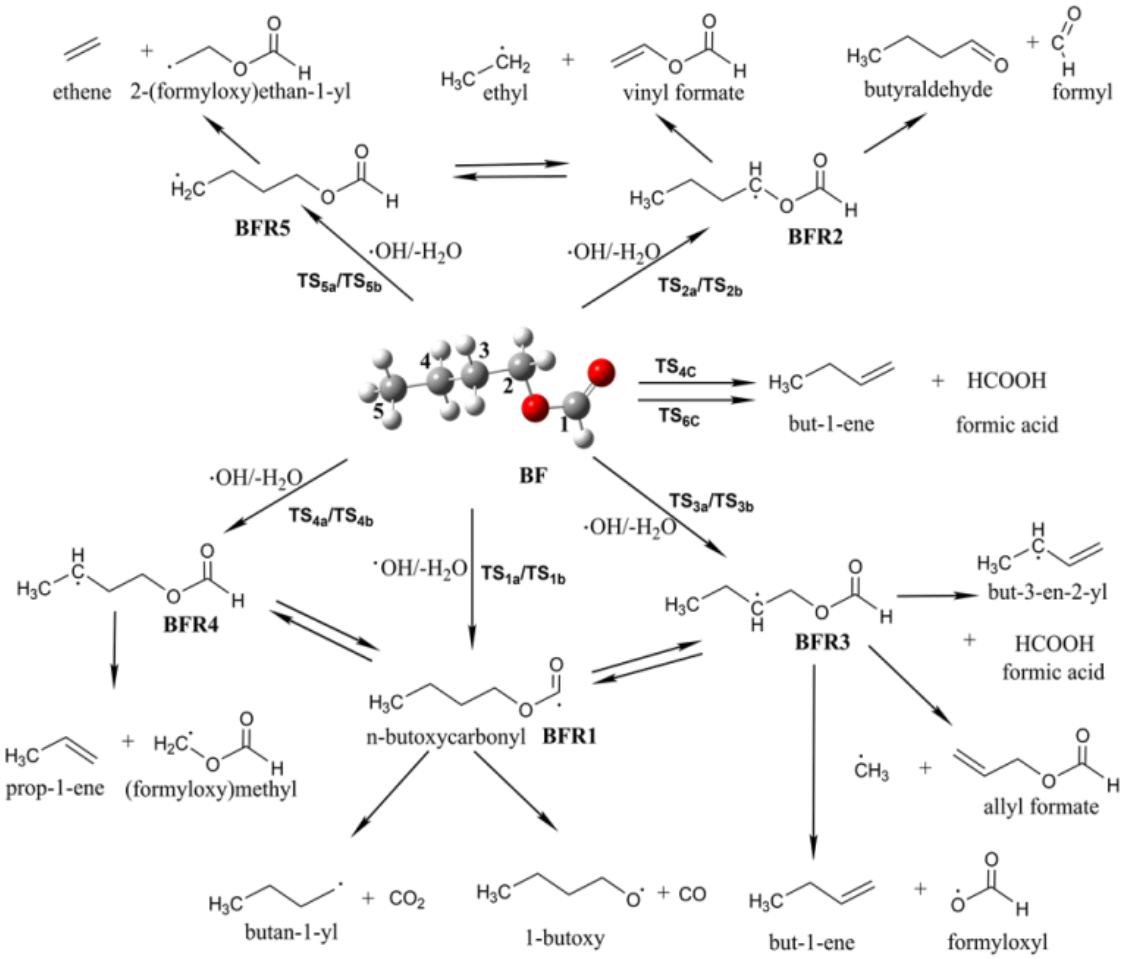

Figure 1: Carbon numbering for butyl formate and chemical pathways for which a rate constant was computed.

Geometry optimization and vibrational frequency calculations were carried out at the MP2/aug-cc-pVDZ [14, 15] level of theory. Each structure was treated using the rigid rotor-harmonic oscillator approximation while the harmonic MP2/aug-cc-pVDZ frequencies were scaled by a factor of 0.959 according to the CCCBDB database [16]. Such scaling of the harmonic wavenumbers is applied in order to include the effect of anharmonicity and reproduce effectively the corresponding experimental values. In accordance with G3 thermochemistry protocol a sequence of single-point energy calculations were applied on the optimized structures [17]. Vibrational analysis was also performed to verify that each transition state (TS) structure demonstrates a unique imaginary frequency, corresponding to the proper reaction coordinate. Intrinsic reaction coordinate (IRC) calculations were also performed at the MP2/aug-cc-pVDZ level of theory to ensure that the transition states lead to the appropriate reactant (RC) and product (PC) complexes. Once the transition states (e.g. TSi) were verified, rate coefficients ($k_i(T)$) were calculated by canonical transition state theory (TST) using the KiSThelP [18] program.

The modified Arrhenius expressions ($k(T) = A \times \mathrm{T}^n \times e^{-E_a/RT}$) resulting from the best fit to the calculated rate constants obtained from 500 to 1300 K are given for each reaction. All species were assumed to be in the electronic ground state, except OH for which the electronic partition function was calculated with a spin orbit splitting of 139.7 cm^{-1} [19]. All electronic structure calculations were carried out with the Gaussian 09 program suite [20]. Finally, the standard enthalpy of formation for BF ($\Delta_f H_{298.15K}{}^0(BF)$) was also calculated using different composite models (CBS-QB3 [21], G3B3 [22] and G3//MP2/aug-cc-pVDZ) by atomization scheme as well as isomerization reaction of ethyl propanoate to BF.

3. Computed rate constants and thermochemistry

3.1.Thermochemical properties of n-butyl formate (BF)

Calculations with different levels of theory and methodologies were carried out in order to characterize the standard enthalpy of formation of n-butyl formate ($\Delta_f H_{298.15K}{}^0(BF)$). The calculated G3B3, G3//MP2/aug-cc-pVDZ and CBS-QB3 values are given in Table 1. G3B3 and G3//MP2/aug-cc-pVDZ differ from each other by the level of theory used for geometry optimization and frequency calculation (B3LYP/6-31G(d) and MP2/aug-cc-pVDZ, respectively). As shown in Table 1, such replacement does not affect the calculated standard enthalpy of formation of n-butyl formate. Using different estimation of the electronic energy (Petersson's CBS in CBS-QB3 and G3B3) also does not change significantly the $\Delta_f H_{298.15K}{}^0(BF)$ value. In addition, $\Delta_f H_{298.15K}{}^0(BF)$ values derived by two independent methods (atomization scheme and isodesmic reaction) were also found to be consistent with each other. It can therefore be assumed that these results are highly independent of the computational method applied here within the accuracy of these composite methods. For simplicity, the G3//MP2/aug-cc-pVDZ results will be used in the discussion of the kinetics, except indicated otherwise. The recommended $\Delta_f H_{298.15K}{}^0$ value of BF can be given as an average value of the above-mentioned six methods (see Table 1) and its modest uncertainty can be estimated by the standard deviation of the computed $\Delta_f H_{298.15K}{}^0(BF)$ values found in Table 1. To our knowledge, only one $\Delta_f H_{298.15K}{}^0(BF)$ value with significant uncertainty is available from the literature [23]. It is consistent with our recommendation.

Table 1: Standard enthalpy of formation ($\Delta_f H_{298.15K}{}^0$) of n-butylformate (BF) calculated using atomization scheme and isomerization reaction. $\Delta_f H_{298.15K}{}^0$ of ethyl propanoate (EP) is -111.5±0.1 kcal/mol according to Wiberg et al. [24].

Methodology	**Level of theory**	$\Delta_f \boldsymbol{H_{298.15K}}{}^{\boldsymbol{0}}$

		(kcal mol^{-1})
Atomization scheme	G3B3	-104.82
	G3//MP2/aug-cc-pVDZ	-104.68
	CBS-QB3	-104.34
Isomerization reaction: EP → BF	G3B3	-103.82
	G3//MP2/aug-cc-pVDZ	-103.89
	CBS-QB3	-103.78
Recommended	-	-104.22 ± 0.70
DPPIR 801 dataset [25]	-	-102.08 ± 3.05

3.2.Unimolecular decomposition of n-butyl formate

Similarly to ethyl propanoate [25-27], n-butyl formate can decompose via either four- or six-centered transition states (TS4C and TS6C) to but-1-ene and formic acid, as illustrated in Figure 2.

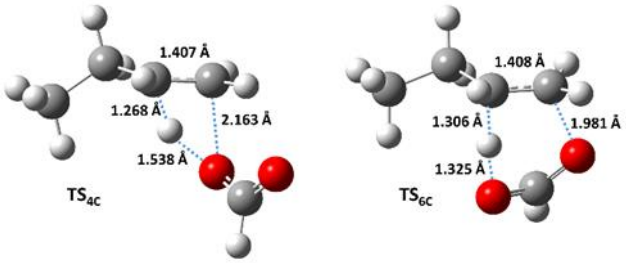

Figure 2: Four- (TS4C) and six-centered (TS6C) transition state structures for the decomposition of butyl formate obtained at the MP2/aug-cc-pVDZ level of theory.

The activation entropy of the BF decomposition is higher for TS4C ($\Delta^{\ddagger}S^{0}_{TS4C}$= 3.36 cal mol^{-1} K^{-1}) than for TS6C ($\Delta^{\ddagger}S^{0}_{TS6C}$= -2.14 cal mol^{-1} K^{-1}), which yields to an increased pre-exponential factor for BF → TS4C → but-1-ene + formic acid (see Table 2). However, the TS4C channel has only a small contribution (less than 5% at 1300K) to the overall decomposition rate due to its remarkably higher activation energy. Therefore, temperature dependence of the overall decomposition at high pressure is almost identical to the rate expression of the TS6C reaction.

Table 2: Fitted parameters for the modified Arrhenius expression for the unimolecular decomposition of BF (500 < *T* (K) < 1300).

BF → C_4H_8-1+HCOOH	A (s^{-1})	n	Ea (kcal mol^{-1})
Through TS4C	3.57×10^{11}	0.95	64.94
Through TS6C	2.43×10^{10}	0.95	50.06

In the case of ethyl propanoate El-Nahas et al. [25] reported CBS-QB3 barrier heights of 66.20 and 50.19 kcal mol^{-1}, in line with our values of 64.27 and 50.03 kcal mol^{-1}, respectively. This rate constant was also measured by Blades et al. [27] and Barnard et al. [26] and the activation energy reported in both these studies is close to 50 kcal.mol^{-1}. The rate constant generally admitted for this ester-type reaction is a combination of the activation energy proposed by El Nahas et al. (50 kcal.mol^{-1}) for ethyl propanoate and the pre-exponential factor of O'Neil and Benson (4×10^{12} s^{-1}) which is sometimes adjusted, as it is the case in the study of Westbrook et al. [7] for small alkyl esters. Our rate constant expression agrees well with these studies as illustrated by Figure 3.

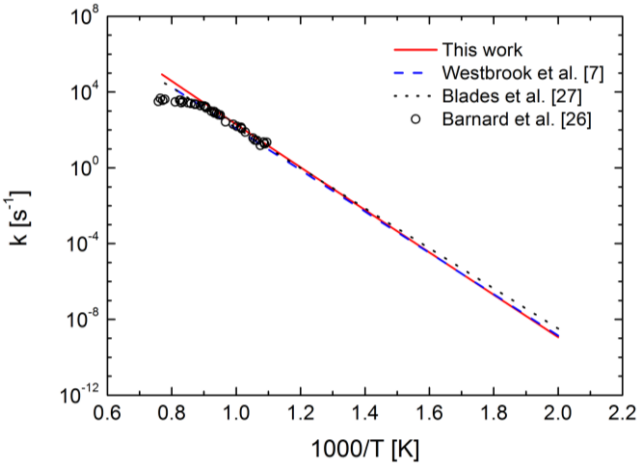

Figure 3: Comparison between rate constants measured for the unimolecular decomposition of ethyl-propanoate [26, 27], a rate constant used by Westbrook et al. for the decomposition of various esters [7] and the rate constant computed in this work for the unimolecular decomposition of butyl formate to formic acid and 1-butene.

Finally, it is worthy to note that the analogous decomposition of ethyl levulinate via six-centered transition state was also investigated by G3MP2//MP2/aug-cc-pVDZ level of theory and the calculated high pressure rate constants of the pyrolysis were in excellent match with corresponding experimental rates [28].

3.3. H-abstraction reactions by OH.

A crucial propagation step in n-butyl formate oxidation is its reaction with the OH radical. According to our IRC calculations at MP2/aug-cc-pVDZ level of theory, H-abstraction from BF by OH radicals can proceed through indirect channels (via pre-reaction complexes, PC) for all the attacked sites, except for the formation of BFR5 radical (4-formyloxy-but-1-yl). Interestingly, only two distinguishable pre-reaction complexes were found, noted as PCa and PCb (Figure 4). The important steps of these reactions can be given as follows (formation of the post-reaction complexes is excluded since the exoergicity of these reactions makes their formation not rate-limiting):

$$BF + OH \overset{K_{IIa}}{\longleftrightarrow} PCa \overset{k_{IIb}}{\longrightarrow} BFRn + H_2O \qquad \text{(n=2)} \qquad (2)$$

$$BF + OH \overset{K_{IIIa}}{\longleftrightarrow} PCb \overset{k_{IIIb}}{\longrightarrow} BFRn + H_2O \qquad \text{(n=1, 3, 4)} \qquad (3)$$

By assuming equilibrium between the bimolecular reactants and the pre-reaction complexes for these indirect H-abstraction reactions, the rate coefficients of reactions 2 and 3 can be expressed in the form $k_{II} = K_{IIa}k_{IIb}$ and $k_{III} = K_{IIIa}k_{IIIb}$, respectively. From statistical thermodynamics and canonical transition state theory, it can be formulated technically equivalent to the bimolecular TST rate expression. This simple kinetic model for reactions with slightly quasi negative activation barrier is able to reproduce experimental rate constants for combustion [29]. One of the reasons for the success of this simple model is that the inner H-abstraction TS is the bottleneck of the reaction due to its tight characteristic compared to the loose characteristic of the PC formation elementary step. Yet, the relative energy of the TS is close to that of the reactants. Furthermore, the use of canonical transition state theory for such reactions is only appropriate if the reaction system is already at high pressure limit. Otherwise RRKM/Master equation calculation is needed to describe the pressure-dependence of the system. Since our aim is to model the reaction system at high pressure condition and no experimental pressure dependent rate constants available for this system, the canonical TST is a reasonable trade-off.

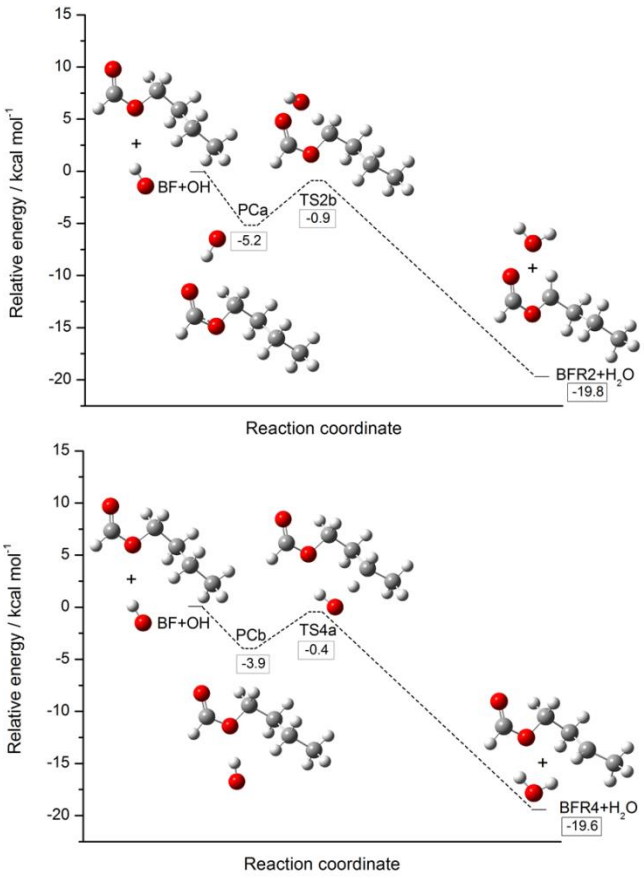

Figure 4: G3//MP2/aug-cc-pVDZ potential energy diagram (including scaled zero-point energies) of two indicative indirect H-abstraction channels of n-butyl formate + OH reaction (via TS2b and TS4a).

Figure 4 shows the effect of the two above-mentioned pre-reaction complexes PCa and PCb on the potential energy surface for the oxidation of BF by OH which yields BFR2 and BFR4, respectively. The presence of attractive interactions between H and O atoms in these pre-reaction complexes remains in the transition state structures. Indeed, this lowers significantly the potential energy of the transition states compared to the direct TS (see Table 3), manifesting in slightly pseudo-negative energy barriers relative to the reactants.

Table 3: Zero-point corrected energies (ΔE_0) and entropies (ΔS^0 at P = 1 atm and T = 298.15 K) for the H-abstraction transition states relative to the energy level of the reactants at the G3//MP2/aug-cc-pVDZ level of theory.

TS		**ΔE_0 (kcal mol^{-1})**	**ΔS^0 (cal mol^{-1} K^{-1})**
TS_{1a}	indirect *via* PCa	1.43	-27.2
TS_{1b}	direct	1.56	-26.1
TS_{2a}	indirect *via* PCa	-1.13	-31.6
TS_{2b}	indirect *via* PCa	-0.89	-31.4
TS_{3a}	indirect *via* PCb	0.25	-30.2
TS_{3b}	direct	1.17	-26.5
TS_{4a}	indirect *via* PCb	-0.44	-30.6
TS_{4b}	direct	0.03	-26.7
TS_{5a}	direct	1.98	-26.0
TS_{5b}	direct	2.82	-25.4

Amongst the above mentioned H-abstractions, the formation of BFR2 can only occur via indirect channels, whereas that of the other BFR radicals are also correlated with transition states corresponding to direct reaction pathways:

$$BF + OH \xrightarrow{k_{IV}} BFRn + H_2O \qquad \text{(n=1, 3, 4, 5)} \quad (4)$$

Therefore, the total bimolecular rate constants for the formation of the BFRn (k_n) were calculated as the sum of all the different transition states located at the same carbon site (n). Figure 5 shows that the G3//MP2/aug-cc-pVDZ calculated overall rate constant at 298 K (1.98×10^{12} cm^3 mol^{-1} s^{-1}) is in excellent agreement with the experimental value of Le Calvé et al. [12] at 298 K (2.13×10^{12} cm^3 mol^{-1} s^{-1}) as well as with the value reported by Wallington et al. [13] at 296 K (1.88×10^{12} cm^3 mol^{-1} s^{-1}). In addition, the G3//MP2/aug-cc-pVDZ calculated rate constants are similar to the experimental data of Ref.12 in the 253–371K temperature range. The best fit to the calculated G3//MP2/aug-cc-pVDZ overall rate constant for BF + OH ($k^{G3}_{BF+OH,ov}(T)$) between 500 K and 1300 K is:

$$k^{G3}_{BF+OH,ov}(T) = 7.61 \times 10^{0}\ (T/K)^{4.00}\ exp(\frac{2.03kcal/mol}{RT})\ cm^3mol^{-1}s^{-1}$$

Vranckx et al. [10] estimated the H-abstraction rate constants of BF based on a comparison with the H-abstraction reactions OH + ethyl formate and OH + n-butanol. Figure 5 shows that these estimated rate constants are lower than our calculated G3//MP2/aug-cc-pVDZ values by a factor of 1.18 at 500 K and 3.34 at 1300 K.

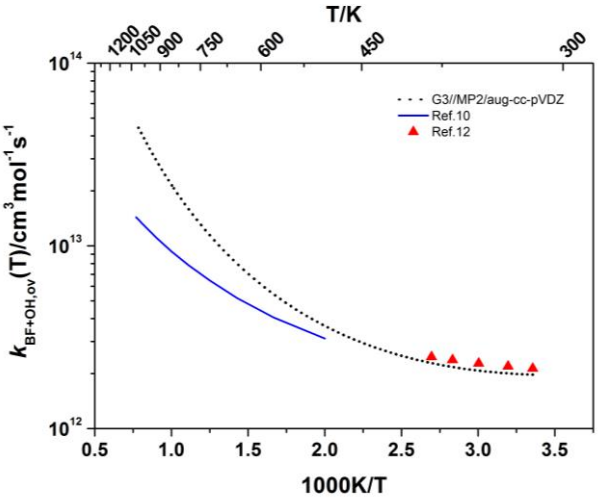

Figure 5: Temperature dependence of the total rate constant for H-abstraction from n-butyl formate (BF) by OH radical. The bimolecular rate constants are calculated by TST from

G3//MP2/aug-cc-pVDZ (dotted lines) level of theory. Blue solid line stands for estimated values from Vranckx et al. [10]. Symbols represent experimental values of Le Calvé et al. [12].

Over the lower temperature range (T<850 K) H-abstraction from the position 4 dominates resulting in the formation of the secondary carbon radical BFR4 (4-formyloxy-but-2-yl) as can be observed in Figure 6. This is clearly due to the low activation barrier, which is the consequence of the strong intermolecular interaction between the hydrogen of the hydroxyl radical and the ether oxygen of the butyl formate in the TS4 transition state structures. Similar interactions had also been identified in the case of other ether + OH and ester + OH reaction systems [30]. The contribution of this process to the overall rate constant changes from 37% to 26% by increasing temperature from 500 K to 850 K. Due to the channel switching at 850 K, the BFR5 (4-formyloxy-but-1-yl) formation becomes the main channel, while the H-abstraction from the ester site of BF producing BFR1 (n-butoxycarbonyl) becomes the second major channel above 1075 K. Their branching ratios at 1100K are 30% and 25%, respectively. The formation of BFR2 (1-formyloxy-but-1-yl) or BFR3 (1-formyloxy-but-2-yl) never exceeds 20 % of the overall rate constant in the temperature range studied. For all of these competing H-abstraction channels, the fitted Arrhenius parameters are given in Table 4.

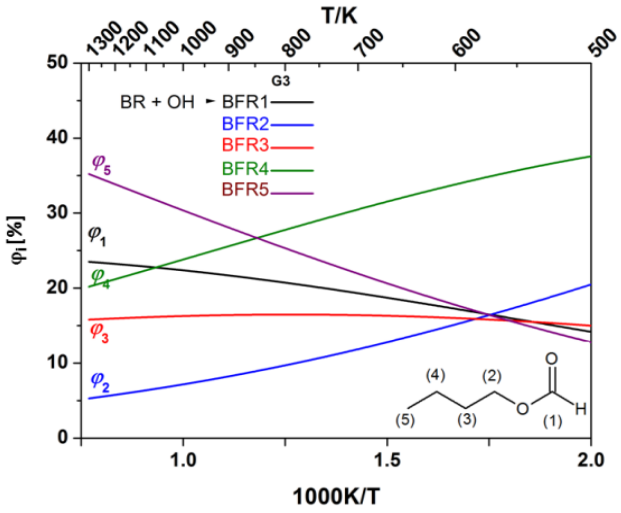

Figure 6: Temperature dependence of the relative branching ratios (φ_i) in percentage for the five H-abstraction channels on n-butyl formate (BF) by OH radical. The bimolecular rate constants are calculated by TST from G3//MP2/aug-cc-pVDZ level of theory.

Table 4: Modified Arrhenius fitted parameters for the total hydrogen abstraction rate constants (k(T)) from n-butyl formate (BF) by OH radical (500K < T < 1300K).

k_n	Reaction	A $cm^3\ mol^{-1}\ s^{-1}$	n	Ea $kcal\ mol^{-1}$
k_1	BF+ OH → BFR1 + H_2O	5.31×10^3	3.01	0.31
k_2	BF+ OH → BFR2 + H_2O	7.82×10^2	2.91	-2.55
k_3	BF+ OH → BFR3 + H_2O	7.28×10^2	3.18	-0.68
k_4	BF+ OH → BFR4 + H_2O	3.42×10^3	2.96	-1.43
k_5	BF+ OH → BFR5 + H_2O	7.02×10^3	3.07	1.04

3.4.Unimolecular decomposition of the fuel radicals

As shown at the top left panel of Figure 7, the rate constant of the decomposition of BFR1 to CO_2 and 1-butyl radical is at least one order of magnitude larger than the other competing consecutive channels, including its isomerization to BFR3 and BFR4. Along with the fact that the H-abstraction reaction on BF by OH leading to BFR1 has one of the largest rate constants above 1100K (φ_1 in Figure 6), this highlights the importance of this two-steps process leading to CO_2. It is worth mentioning that CO formation from BFR1 (Figure 7) is a significant reaction at higher temperatures (i.e. >700K).

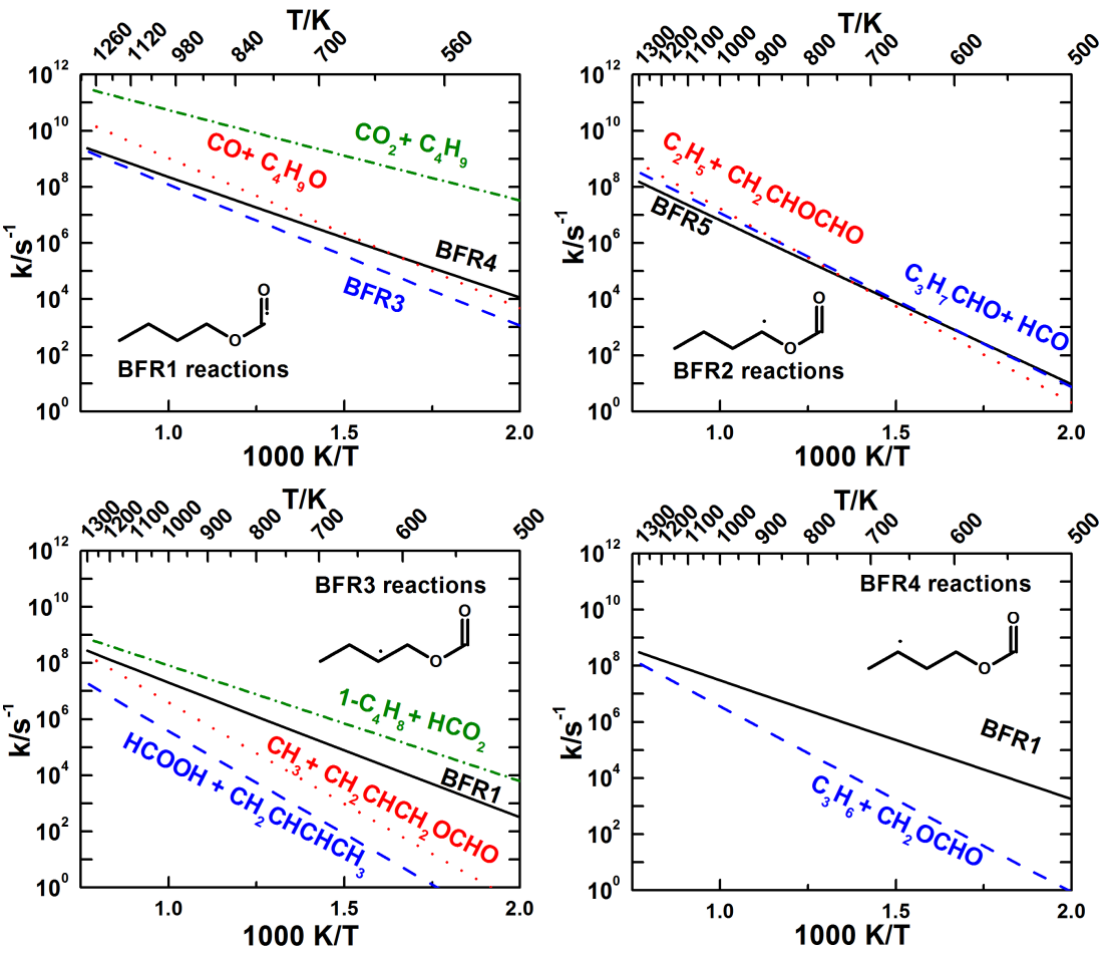

Figure 7: Temperature dependence of the unimolecular rate coefficients (k) of n-butyl formate radicals (BFRn, where n=1–4)

Reaction channels for BFR2 are presented in the top right panel of Figure 7. The rate constants for C–C and C–O bond cleavages of BFR2 (producing C_2H_5 + $CH_2CHOCHO$ and C_3H_7CHO + HCO, respectively) as well as that for its isomerization to BFR5 are comparable over the entire temperature range considered. These channels are of minor importance due to the slower rate constant for the formation of BFR2 by H-abstraction from BF by OH radical (Figure 6).

The formation of BFR3 (φ_3 in Figure 6) from BF is also a minor channel compared to other H-abstraction channels, but the BFR3 radical can isomerize to BFR1 via fast H-shift. As can be seen from the bottom left panel of Figure 6, the corresponding rate coefficient is about one third of the competing decomposition pathway yielding to the formation of 1-butyne and formyloxyl

radical (HCO_2), which dominates over the entire temperature range studied. Other decomposition channels (CH_3 + CH_2CHCH_2OCHO and HCOOH + $CH_2CHCHCH_3$) are kinetically insignificant.

The major H-abstraction channel below 825 K is the formation of BFR4 (φ_4 in Figure 6), but BFR4 isomerizes to BFR1 rather than decomposing to propene and the formyloxymethyl radical (CH_2OCHO), as illustrated in the bottom right panel of Figure 7. The rate constant of the isomerization is found to be faster by more than a factor of 3 compared to the unimolecular decomposition rate constant yielding to the formation of C_3H_6 and CH_2OCHO even at high temperatures.

As can be seen from Figure 6, the formation of BFR5 from BF becomes the most important H-abstraction channel above 850 K. Its isomerization to BFR2 by a 1,4-H-shift also dominates over decomposition to ethylene and 2-formyloxy-eth-1-yl (CH_2CH_2OCHO) radical in this temperature range. The rate constant for the BRF5 to BFR2 isomerization is smaller only at higher temperatures (T>1000K). The fitted Arrhenius parameters for these consecutive unimolecular reactions are given in Table 5.

Table 5: Modified Arrhenius fitted parameters for the unimolecular reactions of the BFRn radicals (500K < T < 1300K).

Reactions	A (s^{-1})	n	Ea (kcal mol^{-1})
Isomerizations			
BFR1 → BFR4	1.79×10^{10}	0.73	18.7
BFR4 → BFR1	1.48×10^{10}	0.47	18.7
BFR1 → BFR3	6.37×10^{10}	0.69	22.0

BFR3 → BFR1	3.66×10^{10}	0.47	21.3
BFR2 → BFR5	5.88×10^{10}	0.57	25.9
BFR5 → BFR2	6.69×10^{10}	0.46	23.3
Decompositions			
BFR1 → CO + butoxy radical	2.08×10^{13}	0.32	24.1
BFR1 → CO_2 + 1-butyl radical	2.39×10^{12}	0.48	14.0
BFR2 → butanal + formyl radical	6.46×10^{12}	0.14	28.2
BFR2 → ethyl + vinyl formate	2.28×10^{12}	0.54	30.9
BFR3 → 1-butyne + formyloxyl radical	2.57×10^{11}	0.19	18.6
BFR3 → formic acid + but-2-en-1-yl radical	1.48×10^{10}	0.80	32.1
BFR3 → methyl radical + allyl formate	7.75×10^{11}	0.57	32.0
BFR4 → propene + (formyloxy)methyl radical	6.89×10^{11}	0.40	29.7
BFR5 → ethene + 2-(formyloxy)ethan-1-yl radical	3.75×10^{12}	0.37	30.1

4. Modeling

The BF sub-mechanism published by Vranckx et al. [10] was taken as a basis and modified with the computed rate constants discussed in the previous section (Unimolecular decomposition of BF, H-abstraction reactions by OH, isomerizations and β-scissions of the fuel radicals). Rate constants computed by Kopp et al. [11] for H-abstraction reactions on BF by H and HO_2 were also included. The unimolecular decomposition of BF yields formic acid (HCOOH), an intermediate expected to be important. A sub-mechanism for this compound based on high-level calculations and on data from the literature was therefore added to the mechanism. The low temperature chemistry of BF was taken from Vranckx et al. [10], however the rate constant used in this study for the unimolecular decomposition of ketohydroperoxyde is $4\times10^{15}\exp(-43000/RT)$ [31], instead of $1\times10^{16}\exp(-39000/RT)$ to stay consistent with the

literature. The addition reactions of the fuel radicals on O_2 were written irreversible both in the forward and reverse direction in the case of Vranckx et al. [10]. This resulted in a reactivity excess with our mechanism and we therefore decided to write it reversible in the forward direction. Thermochemistry of the fuel and its radicals was obtained from calculations at the G3//MP2/aug-cc-pVDZ level of theory. This sub-mechanism was added to a C_0-C_4 core mechanism [32] that includes chemistry for linear alkanes, alkenes, for ketones going up to butanone, for alcohols ranging from methanol to butanol and for aldehydes ranging from formaldehyde to butanal. This mechanism of 376 species involved in 2396 reversible reactions was finally used to simulate experiments in a jet-stirred reactor. These simulations were carried out with the Perfectly Stirred Reactor (PSR) code [33] of the Chemkin II package [34]. Ignition delays were also simulated using SENKIN [35] assuming the constant volume approximation could be used.

5. Experimental apparatus

The oxidation of butyl formate was studied in a fused silica jet-stirred reactor (JSR). Three mixtures of different equivalence ratios (φ = 0.45, 0.9 and 1.8) were considered with a constant initial fuel mole fraction of 900 ppm. This high dilution prevents high heat release within the reactor. Experiments were carried out at 10 atm and the reactants flow rates were adjusted at each temperature to reach a constant residence time of 700 ms [36, 37]. The liquid fuel (from Sigma Aldrich CAS n°592-84-7 – purity ≥ 97%) was handled by a HPLC pump and brought to a two-stage vaporizing system. Butyl formate was first pushed by a nitrogen flow to an annular injector and the resulting spray was vaporized in a heated chamber. A quartz capillary then led the fuel-nitrogen mixture to the entrance of the reactor, where it met the oxidizing mixture (N_2+O_2). Mixing was finally ensured by high turbulence produced by four nozzles and a steady state was quickly reached. The reactor was heated up to 1250 K by two furnaces and the

temperature was measured by a 0.1 mm Pt-Pt/Rh-10% thermocouple protected by a thin wall quartz housing. Gases were sampled by a low pressure sonic probe to freeze the chemical reactions. They were then analyzed online by Fourier transform infrared spectroscopy and stored at low pressure into Pyrex bulbs. Further GC/MS or GC/FID analyses were also carried out on these samples, which were transferred inside a heated piston and pressurized prior to injection, to increase the sensitivity and prevent any condensation issues. Carbon balance was checked at the end of the experiments and was found to be within 10%. Species measured were butyl formate, O_2, H_2O, CO, CO_2, H_2, methane, propene, 1-butene, 1,3-butadiene, acetylene, butanol, acrolein, formic acid, ethylene, acetaldehyde, butanal, and formaldehyde. The uncertainty on species mole fractions is estimated to be ca. 15% based on uncertainties on the analytical measurements, temperature measurements (less than 10 K), pressure measurement (± 0.1 atm), the residence time (less than 5%) and on inlet concentrations of the reactants (less than 5%).

6. Experimental and modeling results

The mole fraction profiles obtained for the different mixtures are illustrated by Figures 8–10. Simulations with the mechanism of Vranckx et al. [10] and the present mechanism are also presented (lines). Butanol was identified as an impurity in the fuel, but in low concentrations and is therefore not expected to interfere strongly with BF chemistry. Butanol was, however, included as a reactant in the simulations ("pC_4H_9OH"). Cool-flame and Negative Temperature Coefficient (NTC) were observed for both lean mixtures, with a bigger amplitude at $\varphi = 0.45$ (Figures 8 and 9). This is illustrated by the fuel profile: consumption starts at 600 K and increases with temperature until 650 K. The fuel consumption then decreases as temperature rises. As the top right panel of Figures 8 and 9 shows, the peak of fuel consumption in the low temperature region (600 – 750 K) corresponds to 200 ppm at $\varphi = 0.9$ and 250 ppm at $\varphi = 0.45$.

The major oxygenated intermediate is formic acid, with maximum concentrations of 150, 300, and 600 ppm for φ = 0.45, 0.9 and 1.8. Other oxygenated intermediates are mainly aldehydes (formaldehyde, acetaldehyde, acrolein, and butanal), and important concentrations of alkenes (mainly ethylene and 1-butene) were also observed.

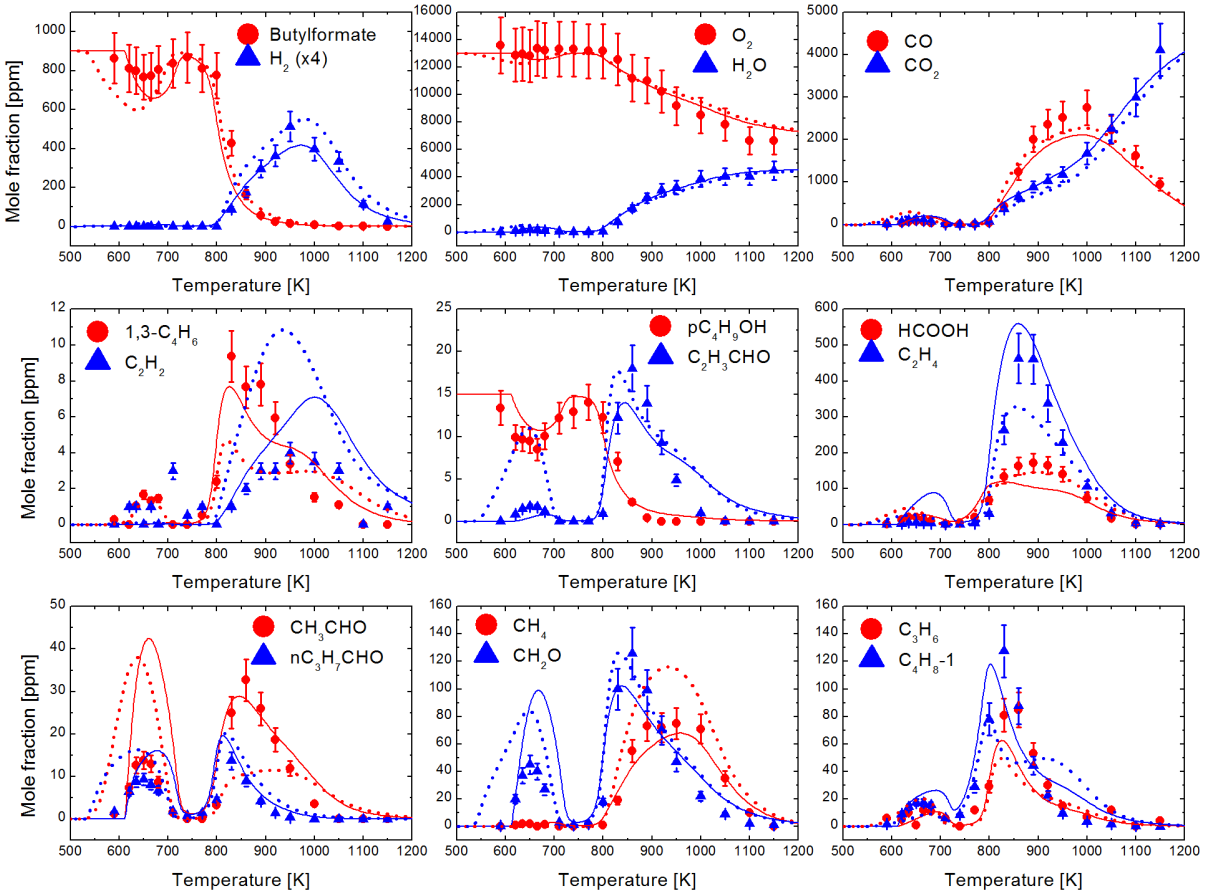

Figure 8: Experimental (symbols) and simulated (lines) mole fraction profiles obtained from the oxidation of butyl formate in a JSR at φ = 0.45 (X_{BF} = 900 ppm and X_{O2} = 13000 ppm), *p* = 10 atm, and τ = 0.7s. Solid line: present mechanism, dotted line: Vranckx et al. [10].

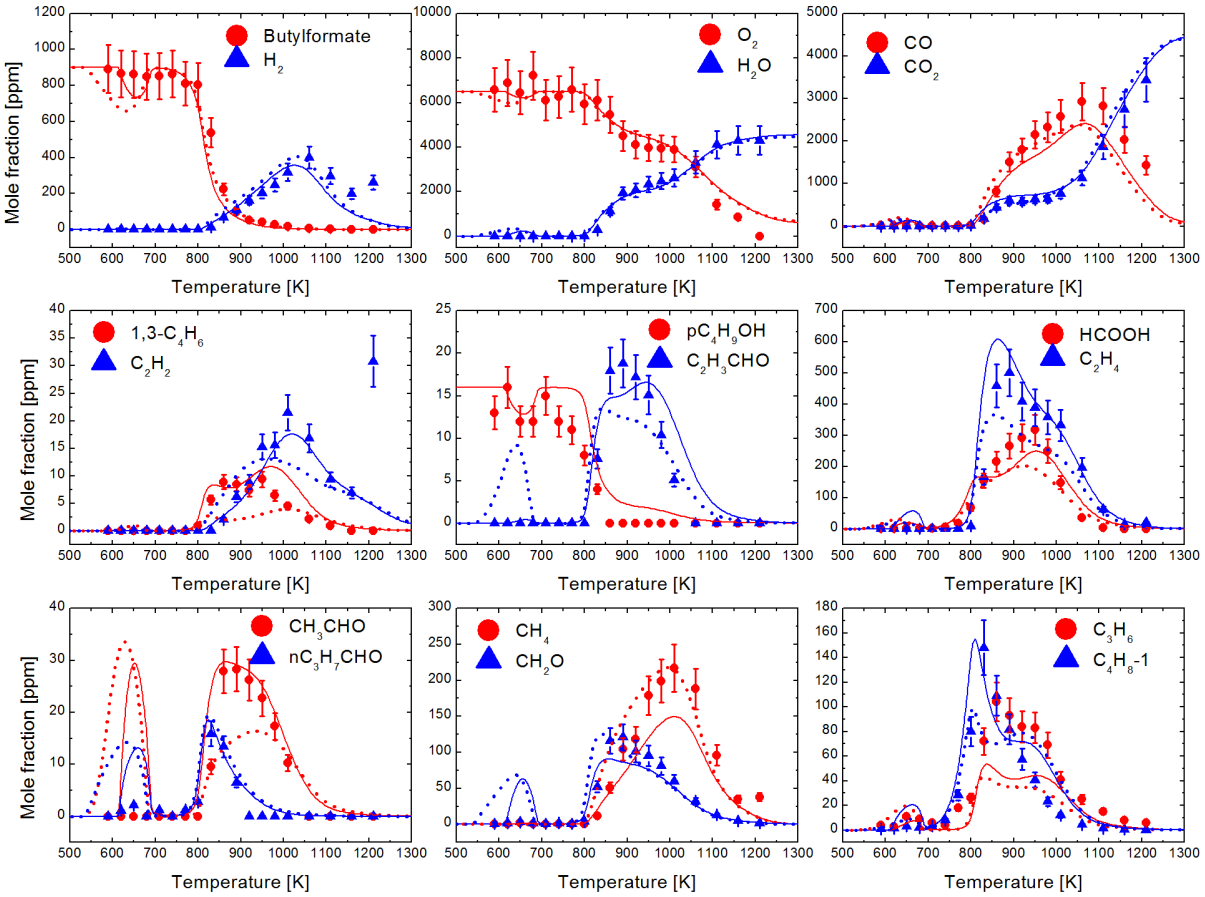

Figure 9: Experimental (symbols) and simulated (lines) mole fraction profiles obtained from the oxidation of butyl formate in a JSR at φ = 0.9 (X_{BF} = 900 ppm and X_{O2} = 6500 ppm), *p* = 10 atm, and τ = 0.7s. Solid line: present mechanism, dotted line: Vranckx et al. [10].

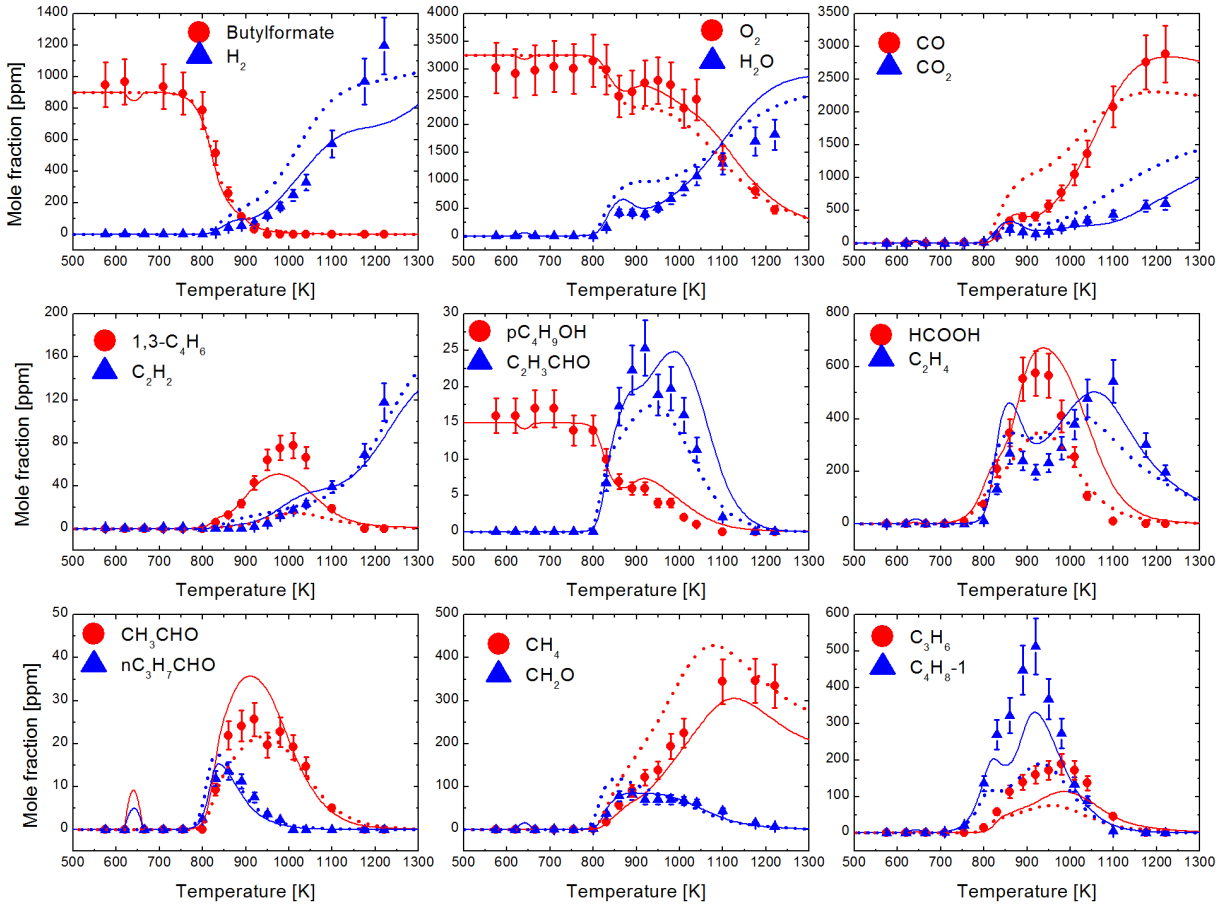

Figure 10: Experimental (symbols) and modelled (lines) mole fraction profiles obtained from the oxidation of butyl formate in a JSR at φ = 1.8 (X_{BF} = 900 ppm and X_{O2} = 3250 ppm), *p* = 10 atm, and τ = 0.7s. Solid line: this work, dotted line: Vranckx et al. [10].

The fuel consumption in the high temperature region is well reproduced by both mechanisms for all fuel mixtures studied. It is important to mention that the present mechanism performs better than that of Vranckx et al. [10] for acetaldehyde, 1-butene and ethylene profiles at high temperature. For instance, acetaldehyde mole fraction obtained using the literature mechanism is under-estimated by a factor of 2 in fuel-lean conditions (φ = 0.45 and 0.9), however it matches well the experimental data under fuel-rich conditions (φ = 1.8). Simulations based on our mechanism fits well the data at φ = 0.45 (Fig. 8) and φ =0.9 (Fig. 9), but it over-estimates the

acetaldehyde profile under fuel-rich conditions. Furthermore, small species (CH_4) and end products (CO, and CO_2) are overestimated by the model of Vranckx et al. [10] at φ = 1.8, which shows too fast consumption of heavier intermediates like 1-butene.

The fuel consumption in the low temperature region is over-estimated by the model of Vranckx et al. [10]. The same observation can be made for the mechanism presented here, but to a lesser extent. This is also reflected by formaldehyde or acetaldehyde profiles which are over-estimated by the model in the 600–700 K temperature interval, as seen in Figure 9. The low temperature reactivity of BF was investigated by means of a rate of production analysis (ROP) on the hydroxyl radical at 660 K for the leaner mixture (φ = 0.45), as OH is the most important species involved during the oxidation of a hydrocarbon and a good reactivity tracer. The results of the present ROP analysis shows that the discrepancies observed between the simulation and the experimental data in the low temperature region could stem from the low temperature chemistry of the butyl radical, as illustrated by Figure 11. A simulation was run without the fuel low-temperature reactions, with no significant alterations of the simulation, which shows that the reactivity is not dependant on these reactions.

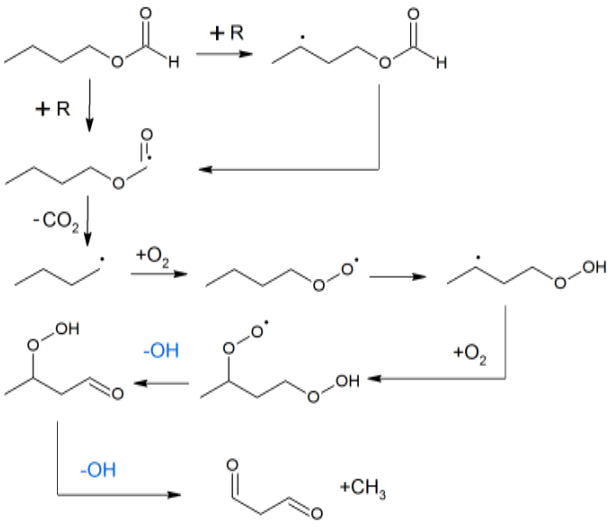

Figure 11: Reaction sequence responsible for the low temperature reactivity observed with the fuel lean mixtures (φ = 0.45 and 0.9) at 660 K.

At high temperature, the main differences in terms of predictions between the two mechanisms can be observed in fuel rich conditions although the fuel consumption is very similar for both models. This is also emphasized by the 1-butene profile in Figure 1 (left bottom panel) which is under-estimated by a factor of two by the model of Vranckx et al. [10]. The experimental data show a dramatic change in reactivity between 800 and 950 K, as illustrated by the bimodal C_2H_4 concentration profile (middle right panel of Figure 10) which peaks at 850 K and 1050 K. Both mechanisms manage to reproduce this trend, but the model we propose shows sharper inflections, in agreement with the data. Pathway analyses at different temperatures were performed to explain this unusual behavior (Figure 12).

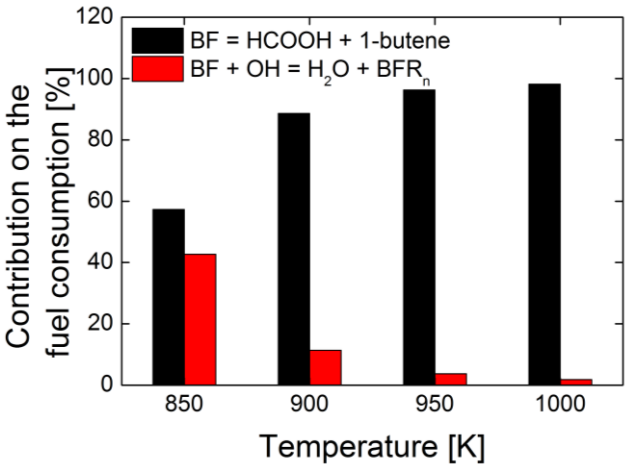

Figure 12: Relative contribution on the fuel consumption for the main reactions involved in BF oxidation from a pathway analysis in fuel rich conditions.

As can be seen from Figure 12, the fuel is mainly consumed by H-abstraction reactions by OH and through unimolecular decomposition producing formic acid and 1-butene. At 850 K, the H-abstraction reactions on BF are competitive and ethylene is mainly formed by the following sequence:

BF + OH = BFR1 + H_2O

$BFR1 = C_4H_9 + CO_2$

$C_4H_9 = C_2H_5 + C_2H_4$

The unimolecular decomposition of the fuel becomes more significant above 850 K, rationalizing the drop of the C_2H_4 and CO_2 profiles. 1-butene and formic acid concentration profiles then increase until a temperature of 900 K is reached. The unimolecular decomposition of the fuel then becomes by far the most important fuel consumption pathways and C_2H_4 is mainly produced from 1-butene via the addition-elimination reaction $1\text{-}C_4H_8 + H = C_2H_5 + C_2H_4$. The ethylene profile finally rises until 1-butene is entirely consumed. This highlights the importance of the 1-butene and formic acid sub-mechanisms in order to accurately simulate the oxidation of butyl formate.

Figure 13 presents other ROP analyses performed at 850 K (black) and 1000 K (red) under near stoichiometric conditions ($\varphi = 0.9$) and provides more insight into the chemistry of butyl formate. As pointed out before, the fuel is almost entirely consumed by the decomposition reaction at 1000 K while oxidation chemistry of BF dominates at 850 K. The H-abstraction reactions are responsible for 67% of fuel consumption at this temperature. Reactions consuming BF to produce BFR4 and BFR5 both contribute at 18% while the formation of BFR1, BFR3, and BFR2 have a 14%, 11%, and 6% contribution to the fuel consumption, respectively. BFR1 is however the most important fuel radical because its pool is fed by isomerization reactions from BFR3 (52%) and BFR4 (95%). This radical then easily decomposes to CO_2 and the butyl radical, the latter becoming the main source of reactivity through the pathways illustrated in Figure 11.

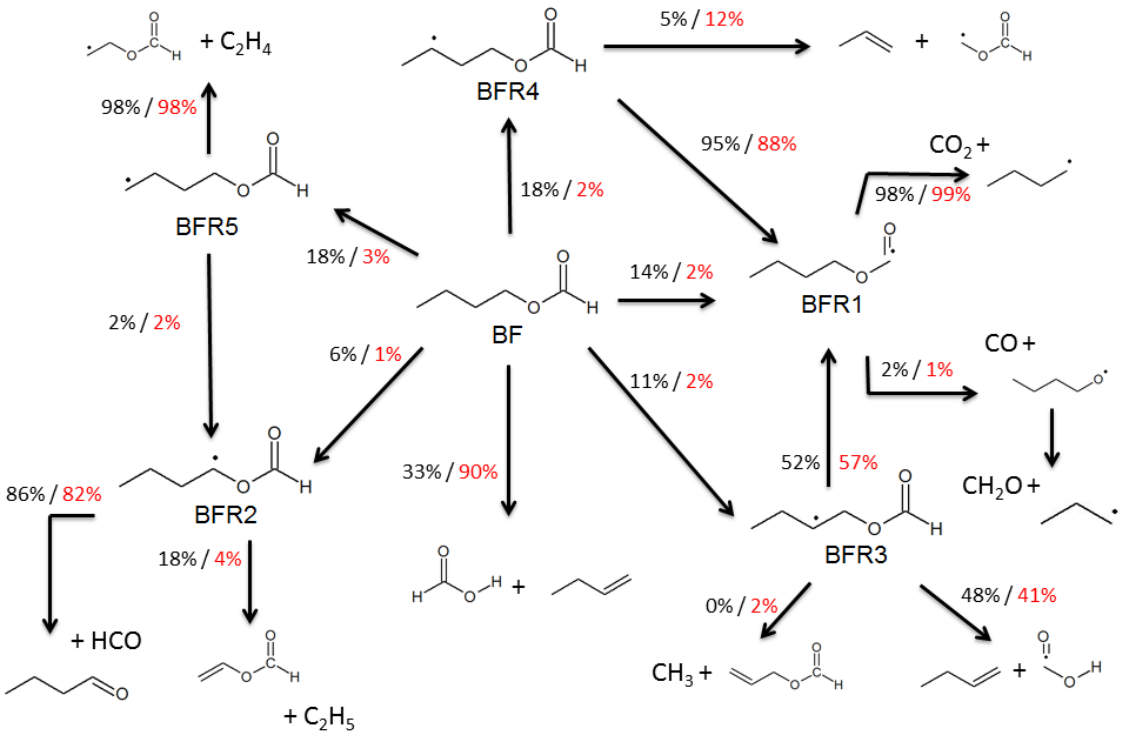

Figure 13: Rate of production analysis obtained with the mechanism presented here at φ = 0.9, 10 atm, 900 ppm of fuel and τ = 0.7s. T = 850 K (black) and T = 1000 K (red).

The mechanism developed here was also used to model high pressure ignition delay times (20 and 90 bar) of a stoichiometric BF/air mixture reported by Vranckx et al. [10] . The simulations with the 2 models were performed using the constant volume approximation as the authors did not provide the volume profiles they used for the modeling. This is illustrated by Figure 14 which shows that the performances of the 2 models are very similar. Discrepancies between the two simulation can however be observed at 20 bar for temperatures below 830 K. This difference between the two mechanisms is mainly due to the rate constant used for the decomposition of the ketohydroperoxydes. This reaction is indeed very sensitive in the temperature region where the two models disagree. Using our rate constant in the mechanism of Vranckx et al. to simulate the experiment at 750 K results in an ignition delay time of 9 ms.

This value is almost twice the prediction of their initial model (5 ms), and is in close agreement with our simulation (11 ms).

The rate constant for such reaction is however not well known and we decided to use a rate constant that was measured for a similar system, and that is commonly recommended for this type of reaction [31] (4×10^{15}exp(-43000/RT)). The rate constant used by Vranckx et al. [10] is faster (1×10^{16}exp(-39000/RT)), which results in more reactivity. This can also be observed on the fuel profile obtained with the JSR for the fuel-lean mixture, where the reactivity is overestimated with the mechanism of the literature. This simulation however validates our model for high pressures as highlighted by the simulation at 90 bar which is very reliable.

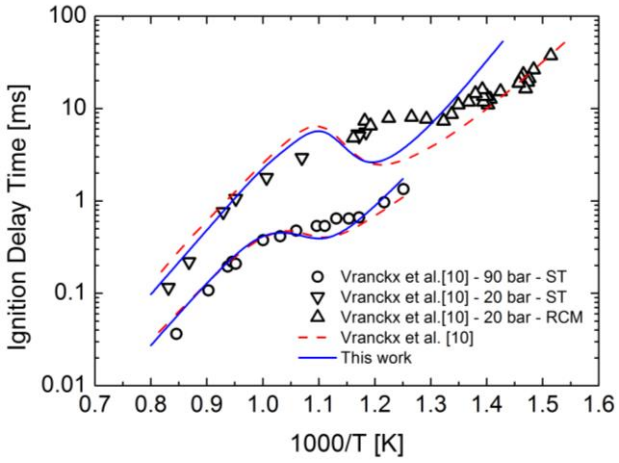

Figure 14: Measured [10] (symbols) and simulated (lines) ignition delay times of BF/air stoichiometric mixtures at 20 and 90 bar in a shock tube and a rapid compression machine. Solid blue line: this work, dashed red line: Vranckx et al. [10]

7. Conclusions

The kinetics of n-butyl formate decomposition was studied by performing *ab initio* calculations and experiments in a jet-stirred reactor. The *ab initio* based rate constant for the unimolecular

decomposition of the fuel to formic acid and 1-butene is comparable to that of other esters [25]. Experiments confirmed that this unimolecular step is one of the major processes governing the oxidation of BF in a jet-stirred reactor. Rate constants for the unimolecular decomposition of the fuel radical and for H-abstraction reactions by OH on the fuel were computed as well. The overall rate expression obtained from G3//MP2/aug-cc-pVDZ calculations is in good agreement with the low-temperature experimental data for BF oxidation by OH [12]. These rate constants were used to develop a detailed mechanism to simulate the oxidation of BF in a jet-stirred reactor.

The agreement between experimental data and simulation is reasonable and a rate of production analysis revealed a competition between the molecular reaction and oxidation by the hydroxyl radical. This competition is responsible for a two steps reactivity that was observed in fuel-rich conditions. Low temperature reactivity was also observed in fuel-lean conditions and the model was able to catch it. A rate of production analysis showed that this reactivity is due to a reaction sequence involved in the low-temperature chemistry of the primary butyl radical.

An approach to improve the mechanism would be to work at higher pressure, or with fuel leaner mixtures. This would inhibit the unimolecular decomposition of the fuel which was a major consumption pathway in our conditions, resulting in a higher contribution from the reactions related to oxidation.

8. Supplementary material

Detailed mechanism and thermodynamic data in the Chemkin format, geometries of the different species at the MP2/aug-cc-pVDZ level of theory used for the calculations.

9. Acknowledgements

The research leading to these results has received funding from the European Research Council under the European Community's Seventh Framework Programme (FP7/2007–2013)/ERC grant agreement No.291049 – 2G-CSafe. Financial support from the Labex Caprysses (convention ANR-11-LABX-0006-01) is gratefully acknowledged. The authors would like to thank László Müller and Máté Labádi for the administration of the computing systems used for this work. Milán Szőri was a Magyary Zoltán Fellow supported by State of Hungary and the European Union, financed by the European Social Fund in the framework of TÁMOP 4.2.4.A/2-11-1-2012-0001 "National Excellence Program" under the respective grant number of A2-MZPD-12-0139. This paper was supported by the János Bolyai Research Scholarship of the Hungarian Academy of Sciences (BO/00113/15/7) and by the Scientific Fund of SZTE JGYPK (CS-009/2015). The authors would also like to thank Professor Eric Henon, from University of Reims Champagne-Ardenne (URCA), for his useful feedback concerning KiSThelP.

10. References

1. Boot, M., et al., *Cyclic Oxygenates: A New Class of Second-Generation Biofuels for Diesel Engines?* Energy & Fuels, 2009. **23**(4): p. 1808-1817.
2. Zaras, A.M., P. Dagaut, and Z. Serinyel, *Computational Kinetic Study for the Unimolecular Decomposition Pathways of Cyclohexanone.* The Journal of Physical Chemistry A, 2015. **119**(28): p. 7138-7144.
3. Thion, S., et al., *Theoretical kinetic study for methyl levulinate: oxidation by OH and CH3 radicals and further unimolecular decomposition pathways.* Physical Chemistry Chemical Physics, 2015. **17**(36): p. 23384-23391.
4. Janssen, A.J., et al., *Tailor-Made Fuels from Biomass for Homogeneous Low-Temperature Diesel Combustion.* Energy & Fuels, 2011. **25**(10): p. 4734-4744.
5. Miyamoto, N., et al., *Smokeless, Low NOx, High Thermal Efficiency, and Low Noise Diesel Combustion with Oxygenated Agents as Main Fuel.* SAE Technical Paper 980506, 1998.
6. Westbrook, C.K., W.J. Pitz, and H.J. Curran, *Chemical Kinetic Modeling Study of the Effects of Oxygenated Hydrocarbons on Soot Emissions from Diesel Engines.* The Journal of Physical Chemistry A, 2006. **110**(21): p. 6912-6922.
7. Westbrook, C.K., et al., *A detailed chemical kinetic reaction mechanism for oxidation of four small alkyl esters in laminar premixed flames.* Proceedings of the Combustion Institute, 2009. **32**(1): p. 221-228.
8. Dooley, S., et al., *Methyl formate oxidation: Speciation data, laminar burning velocities, ignition delay times, and a validated chemical kinetic model.* International Journal of Chemical Kinetics, 2010. **42**(9): p. 527-549.
9. Dooley, S., et al., *An experimental and kinetic modeling study of methyl formate low-pressure flames.* Combustion and Flame, 2011. **158**(4): p. 732-741.
10. Vranckx, S., et al., *An experimental and kinetic modelling study of n-butyl formate combustion.* Combustion and Flame, 2013. **160**(12): p. 2680-2692.
11. Kopp, W.A., et al., *Hydrogen Abstraction from n-Butyl Formate by H• and HO2•.* The Journal of Physical Chemistry A, 2013. **117**(31): p. 6757-6770.
12. Le Calvé, S., G. Le Bras, and A. Mellouki, *Temperature Dependence for the Rate Coefficients of the Reactions of the OH Radical with a Series of Formates.* The Journal of Physical Chemistry A, 1997. **101**(30): p. 5489-5493.
13. Wallington, T.J., et al., *The gas phase reactions of hydroxyl radicals with a series of esters over the temperature range 240–440 K.* International Journal of Chemical Kinetics, 1988. **20**(2): p. 177-186.
14. Møller, C. and M.S. Plesset, *Note on an Approximation Treatment for Many-Electron Systems.* Physical Review, 1934. **46**: p. 618-622.
15. Kendall, R.A., T.H. Dunning, and R.J. Harrison, *Electron affinities of the first-row atoms revisited. Systematic basis sets and wave functions.* The Journal of Chemical Physics, 1992. **96**: p. 6796-6806.
16. Baldwin, R.R., et al., *Second Limit of Hydrogen+Oxygen Mixtures: the Reaction H+HO2.* Journal of the Chemical Society, Faraday Transactions 1: Physical Chemistry in Condensed Phases, 1974. **70**: p. 635-641.
17. Curtiss, L.A., et al., *Gaussian-3 (G3) theory for molecules containing first and second-row atoms.* Journal of Chemical Physics, 1998. **109**(18): p. 7764-7776.

18. Canneaux, S., F. Bohr, and E. Henon, *KiSThelP: A program to predict thermodynamic properties and rate constants from quantum chemistry results†.* Journal of Computational Chemistry, 2014. **35**: p. 82-93.
19. Herzberg, G., *Molecular Spectra and Molecular Structure, Vol. I: Spectra of Diatomic Molecules*. 2nd ed. ed. 1989, Malabar, FL: Krieger.
20. Frisch, M.J., et al., *Gaussian 09*. 2009: Wallingford CT. p. Gaussian, Inc.,.
21. Montgomery, J.A., et al., *A complete basis set model chemistry. VI. Use of density functional geometries and frequencies.* Journal of Chemical Physics, 1999. **110**(6): p. 2822-2827.
22. Baboul, A.G., et al., *Gaussian-3 Theory Using Density Functional Geometries and Zero-Point Energies.* J Chem Phys, 1999. **110**: p. 7650-7657.
23. Rowley, R.L., et al., *Data Compilation of Pure Compound Properties*. 2001, AIChE: New York, NY.
24. Wiberg, K.B. and R.F. Waldron, *Lactones .2. Enthalpies of Hydrolysis, Reduction, and Formation of the C4-C-13 Monocyclic Lactones - Strain Energies and Conformations.* Journal of the American Chemical Society, 1991. **113**(20): p. 7697-7705.
25. El-Nahas, A.M., et al., *Enthalpies of Formation, Bond Dissociation Energies and Reaction Paths for the Decomposition of Model Biofuels: Ethyl Propanoate and Methyl Butanoate.* The Journal of Physical Chemistry A, 2007. **111**(19): p. 3727-3739.
26. Barnard, J.A., A.T. Cocks, and T.K. Parrott, *Thermal unimolecular decomposition of ethyl propionate behind reflected shock waves.* Journal of the Chemical Society, Faraday Transactions 1: Physical Chemistry in Condensed Phases, 1976. **72**(0): p. 1456-1463.
27. Blades, A.T. and P.W. Gilderson, *KINETICS OF THE THERMAL DECOMPOSITION OF ETHYL PROPIONATE.* Canadian Journal of Chemistry, 1960. **38**(9): p. 1412-1415.
28. AlAbbad, M., et al., *On the high-temperature unimolecular decomposition of ethyl levulinate.* Proceedings of the Combustion Institute, 2017. **36**(1): p. 187-193.
29. Bansch, C., et al., *Reaction of Dimethyl Ether with Hydroxyl Radicals: Kinetic Isotope Effect and Prereactive Complex Formation.* Journal of Physical Chemistry A, 2013. **117**(35): p. 8343-8351.
30. Khaled, F., et al., *A combined high-temperature experimental and theoretical kinetic study of the reaction of dimethyl carbonate with OH radicals.* Physical Chemistry Chemical Physics, 2017. **19**(10): p. 7147-7157.
31. Sahetchian, K.A., et al., *The pyrolysis of organic hydroperoxides (ROOH).* Proceedings of the Combustion Institute, 1992. **24**(1): p. 637-643.
32. Fenard, Y., et al., *Experimental and kinetic modeling study of trans-2-butene oxidation in a jet-stirred reactor and a combustion bomb.* Proceedings of the Combustion Institute, 2015. **35**(1): p. 317-324.
33. Glarborg, P., et al., *PSR: A Fortran Program for Modeling Well-Stirred Reactors*. 1986, Sandia National Laboratories: Albequerque, NM.
34. Kee, R.J., F.M. Rupley, and J.A. Miller, *Chemkin II: A Fortran chemical kinetics package for the analysis of gas-phase chemical kinetics.* Sandia Report, 1989. **SAND89-80009B UC-706**.
35. Lutz, A., R. Kee, and J. Miller, *SENKIN: A FORTRAN Program for Predicting Homogeneous Gas Phase Chemical Kinetics with Sensitivity Analysis.* Sandia Report, 1988. **SAND87-8248 UC-401**.
36. David, R. and D. Matras, *Règies de construction et d'extrapolation des réacteurs auto-agités par jets gazeux.* The Canadian Journal of Chemical Engineering, 1975. **53**(3): p. 297-300.

37. Matras, D. and J. Villermaux, *Un réacteur continu parfaitement agité par jets gazeux pour l'étude cinétique de réactions chimiques rapides.* Chemical Engineering Science, 1973. **28**(1): p. 129-137.

11. List of figures

Figure 9: Experimental (symbols) and simulated (lines) mole fraction profiles obtained from the oxidation of butyl formate in a JSR at φ = 0.9 (XBF = 900 ppm and XO_2 = 6500 ppm), p = 10 atm, and τ = 0.7s. Solid line: present mechanism, dotted line: Vranckx et al. [10].

Figure 10: Experimental (symbols) and modelled (lines) mole fraction profiles obtained from the oxidation of butyl formate in a JSR at φ = 1.8 (XBF = 900 ppm and XO_2 = 3250 ppm), p = 10 atm, and τ = 0.7s. Solid line: this work, dotted line: Vranckx et al. [10].

Figure 11: Reaction sequence responsible for the low temperature reactivity observed with the fuel lean mixtures (φ = 0.45 and 0.9) at 660 K.

Figure 12: Relative contribution on the fuel consumption for the main reactions involved in BF oxidation from a pathway analysis in fuel rich conditions.

Figure 13: Rate of production analysis obtained with the mechanism presented here at φ = 0.9, 10 atm, 900 ppm of fuel and τ = 0.7s. T = 850 K (black) and T = 1000 K (red).

Figure 14: Measured [10] (symbols) and simulated (lines) ignition delay times of BF/air stoichiometric mixtures at 20 and 90 bar in a shock tube and a rapid compression machine. Solid blue line: this work, dashed red line: Vranckx et al. [10].